Mean force between like-charged macroions at high electrostatic coupling

2002 J. Phys.: Condens. Matter 14 13449

(http://iopscience.iop.org/0953-8984/14/49/304)

INSTITUTE OF PHYSICS PUBLISHING JOURNAL OF PHYSICS: CONDENSED MATTER

J. Phys.: Condens. Matter **14** (2002) 13449–13467 PII: S0953-8984(02)38195-5

Mean force between like-charged macroions at high electrostatic coupling

Per Linse

Physical Chemistry 1, Center for Chemistry and Chemical Engineering, Lund University, PO Box 124, S-221 00 Lund, Sweden

E-mail: per.linse@fkem1.lu.se

Received 14 June 2002, in final form 21 October 2002
Published 29 November 2002
Online at stacks.iop.org/JPhysCM/14/13449

Abstract

Interactions between two like-charged macroions in the presence of their counterions confined in a cylindrical cell have been investigated by Monte Carlo simulations. The mean force and the potential of mean force (pmf) as a function of the macroion separation have been determined at conditions at which short-range attractions become significant. As the electrostatic coupling is increased, the nature of the mean force changes from being purely repulsive to being attractive at short separations and finally attractive at all separations. At a sufficiently large electrostatic coupling, the attractive mean force is promoted by an increase of the macroion charge to counterion charge ratio and by an increase of the macroion volume fraction (assuming a not too concentrated solution). At the onset of an attractive force, nearly all counterions are localized at the macroion surfaces, but the counterions still display a two-dimensional fluid structure. The pmfs determined from the cylindrical cell model agreed qualitatively very well with those obtained from simulations of corresponding fluids, suggesting that higher-order macroion correlations are of less importance. Finally, it is argued that the attractive component of the mean force originates from spatial correlations between counterions residing near different macroions.

(Some figures in this article are in colour only in the electronic version)

1. Introduction

The understanding of mechanisms that determine forces between particles is of crucial importance in science as well as in applications. Charged colloidal systems are not an exception here, but rather one of the most important systems since they constitutes, for example, the basis of living cells and are common in pharmacy, food stuff, paints, paper etc.

A major theoretical step for rationalizing colloidal stability was taken in the 1940s when Derjaguin, Landau, Verwey and Overbeek [1, 2] proposed a theory, now known as the DLVO theory, which predicts a purely repulsive electrostatic force between like-charged colloidal particles. In the late 1960s, this view was questioned when Oosawa [3, 4] proposed that like-charged cylindrical objects might display an attraction of electrostatic origin mediated by their counterions. Twenty years later, the classical DLVO theory was more seriously challenged by direct observations of such attractions in simple model systems containing objects possessing planar [5, 6], cylindrical [7] and spherical [8–13] geometry solved with simulations and/or accurate liquid state theories. The attraction appearing in these model studies is all short-ranged and is manifested in different experimental systems [14]. On the basis of advanced statistical–mechanical theories, Kjellander and co-workers explained the attractive component appearing in addition to the repulsive mean-field interaction as originating from spatial correlations between ions residing near different charged planes [15], basically in agreement with Oosawa's suggestion. For general reviews on interactions between charged colloids, see, for example [16–18].

In previous studies, Allahyarov *et al* [9], Grønbech-Jensen *et al* [10] and Wu *et al* [11, 13] examined the mean force and/or the potential of mean force (pmf) between two like-charged macroions in a finite volume containing two macroions and their counterions at different conditions using related approaches. In these studies, conditions were found at which an attractive force was operating at short macroion separation. The properties of the corresponding fluids have also been determined for an extended and connected region of the parameter space described by the three reduced parameters: (i) macroion charge to counterion charge ratio, (ii) the macroion volume fraction, and (iii) an electrostatic coupling parameter, completely describing the system [19, 20]. The fluid conventionally characterized by effective repulsion between macroions was at larger electrostatic coupling replaced by a fluid with short-range attraction between macroions and at sufficiently large coupling the fluid displayed a gas–liquid phase transition. In a later study [21], the effective macroion–macroion pair potential was determined by inverse Monte Carlo (MC) simulation and indeed at certain conditions a short-ranged attractive force was found.

The aim of the present contribution is to investigate the attraction between two like-charged macroions in more detail. The simplified approach of investigating the mean force and pmf between two like-charged macroions in a limited volume containing only two like-charged macroions and their counterions has been taken [9–11, 13]. Here, a cylindrical cell has been adopted and efficient methods to sample the mean force and the pmf has been employed. The values of the three reduced parameters characterizing the system have been varied in a region of the parameter space in which short-range attractions appear. In particular, the mean force and the pmf were evaluated, and thereafter they were related to the observed structure and phase instability of the corresponding fluid, which includes full many-body effects. Moreover, the nature of the attractive force and the role of the spatial correlations of the counterions are discussed.

2. Model

The so-called primitive model is employed, in which the aqueous colloidal solution is represented by a mixture of hard spheres (referred to as macroions) and point-like counterions, interacting with each other only via electrostatic and hard-sphere potentials. The solvent enters the model only through its relative permittivity.

The total potential energy of the system U is assumed to be pairwise additive according to

$$U = \sum_{i<j} u_{ij}. \tag{1}$$

The pair energy u_{ij}, where i and j denote either a macroion (M) or a counterion (I), is given by

$$u_{ij}(r) = \begin{cases} \infty, & r < R_i + R_j \\ \dfrac{Z_i Z_j e^2}{4\pi\varepsilon_0\varepsilon_r}\dfrac{1}{r}, & r \geqslant R_i + R_j, \end{cases} \tag{2}$$

where Z_i is the charge on particle i, R_i the radius of particle i, e the elementary charge, ε_0 the permittivity of vacuum, ε_r the relative permittivity of the solvent and r the centre-to-centre separation between the particles.

The model system is favourably described in reduced units. The complete set consisting of: (i) the macroion charge to counterion charge ratio Z_r, (ii) the macroion volume fraction ϕ_M and (iii) an electrostatic coupling parameter Γ_{II} will be used here.

These parameters are defined according to [19]

$$Z_r \equiv -(Z_M/Z_I), \tag{3}$$

$$\phi_M \equiv (4\pi/3)R_M^3\rho_M, \tag{4}$$

$$\Gamma_{II} \equiv Z_I^2 L_B/R_M, \tag{5}$$

where Z_M is the macroion charge, Z_I the counterion charge, R_M the macroion radius, $\rho_M \equiv N_M/V$ the macroion number density with N_M being the number of macroions and V the volume of the system, and $L_B \equiv e^2/4\pi\varepsilon_0\varepsilon_r kT$ the Bjerrum length with k being the Boltzmann constant and T the temperature. The system contains $N_I = N_M Z_r$ counterions, in total $N = N_M + N_I$ particles and the total number density becomes $\rho = \rho_M + \rho_I$ with $\rho_I \equiv N_I/V$.

In the present investigation, two macroions ($N_M = 2$) and their counterions in a dielectric continuum constituting an electroneutral system will be considered. The charged particles are confined inside a hard-walled cylindrical cell with radius R_{cyl} and length L_{cyl}. The macroions are allowed to explore only positions along the C_∞-symmetry axis of the cylinder (the z axis) and the positions of the particles are centred at $z = 0$ to minimize the effects of the cylinder walls.

The volume V of the cell is related to the macroion number density ρ_M^{fluid} according to $V = 2/\rho_M^{fluid}$. As expected, and also examined in section 6.2, the effective macroion–macroion interaction depends on the cell volume. The cylindrical cell approach employed rests on the assumption that the effective interaction is at most weakly dependent on the shape (R_{cyl}/L_{cyl} ratio) of the cylindrical cell. Given that $L_{cyl}/2$ is larger than the range of the interaction and that R_{cyl} is somewhat larger than R_M, this assumption was found to be correct.

Two different conditions will be considered: (i) Z_r counterions constrained to each surface of the two macroions but the counterions still being mobile on the surface (surface constraint) and (ii) $2Z_r$ counterions able to explore the full cylinder volume V (no constraint). The use of these two conditions will support the conceptual separation of the effective macroion–macroion interaction into different components that we have made below. In the constrained case, the cylinder walls have no influence on the properties of the system. Conceptually, the system is divided into two subsystems separated by the $z = 0$ plane.

3. Mean force and potential of mean force

The force and the corresponding potential acting between the two macroions and mediated by their counterions will be discussed. Since the macroions and their counterions are confined in

a cell, which approximately takes into account the influence of the surrounding electrolyte, the force is a mean force rather than an effective one. In the corresponding fluid, the macroion–macroion mean force is the force acting between two macroions averaged over the positions of surrounding counterions *and* macroions, whereas an N-body effective force among N macroions is averaged over the positions of surrounding counterions only. The latter can be approximated by a pairwise sum of effective pair forces. The same holds for the potential. See also, for example, the review by Belloni [17].

The mean force F operating on one of the macroions, say M, projected on the macroion–macroion inter-particle vector $\boldsymbol{r}_{MM}$ (later simplified by $\boldsymbol{r}$) is defined by

$$F(r) \equiv \sum_{i \neq M}^{N} \langle -\nabla_{r_{Mi}} u_{Mi}(r_{Mi}) \rangle, \tag{6}$$

with $F(r) > 0$ implying a repulsive and $F(r) < 0$ an attractive mean force and $\langle \cdots \rangle$ denoting an ensemble average of the positions of the counterions. The related pmf U^{pmf} is defined by

$$U^{pmf}(r) \equiv -\int_{\infty}^{r} F(r')\,\mathrm{d}r'. \tag{7}$$

At large r, $F(r)$ and $U^{pmf}(r)$ approach zero. Both quantities depend on (i) the direct repulsive macroion–macroion interaction $u_{MM}(r)$ and (ii) an indirect contribution mediated by the counterions.

From a force balance, the mean force can be divided into two terms according to

$$F(r) = F_{ideal}(r) + F_{elec}(r) \tag{8}$$

where

$$F_{ideal}(r) = kT[\rho_I(z=0) - \rho_I(z = L_{cyl}/2)]A \tag{9}$$

$$F_{elec}(r) = \sum_{i<j}^{N}{}' \langle -\nabla_{r_{ij}} u_{ij}(r_{ij}) \rangle, \tag{10}$$

with $F_{ideal}(r)$ arising from the difference in the transfer of linear moments of the counterions across the planes $z = 0$ and $L_{cyl}/2$ and $F_{elec}(r)$ being an average force appearing across the plane $z = 0$ originating from the electrostatic interaction among the charged particles. In equation (9), $\rho_I(z = z')$ denotes the counterion number density in the plane $z = z'$ averaged over the cylindrical cross section with area A, and in equation (10) $'$ in the summation denotes that only pairs of particles located at different sides of the plane $z = 0$ (belonging to different subsystems) should be considered. As long as $r \ll L_{cyl}/2$, $F_{ideal}(r)$ is dominated by the $\rho_I(z = 0)$ term. The pmf can similarly be separated according to

$$U^{pmf}(r) = U^{pmf}_{ideal}(r) + U^{pmf}_{elec}(r). \tag{11}$$

Four additional comments have to be made.

(1) Similar division of the mean force, as in equation (8), has been made for the corresponding planar systems [5, 14, 22]. In that case, two simplifications arise: (i) in equation (9) the density at only one plane appears and (ii) the density is uniform in that plane.

(2) In the limit of r and $L_{cyl} - r$ being sufficiently large to make the interaction between the subsystems and the influence from the cylinder ends weak, $F_{ideal}(r)$ becomes small due to $\rho_I(z = 0)$ and $\rho_I(z = L_{cyl})$ being small. In the present system with attractive macroion–counterion interaction, $F_{ideal}(r)$ becomes repulsive at shorter macroion separation because the counterion density at the mid-plane is larger than that at the cylinder ends. Thus, at not too large r, $F_{ideal}(r)$ denotes the contribution to the mean force acting between

the macroions arising from an excess accumulation of counterions in a plane between the macroions. Naturally, $F_{ideal}(r)$ depends indirectly on the electrostatic interaction in the system, for example for the corresponding uncharged system $F_{ideal}(2R_M < r < L_{cyl} - 2R_M) \equiv 0$.

(3) In the planar geometry, $F_{elec}(r)$ is attractive, whereas in our system with two interacting spherical macroions $F_{elec}(r)$ can be repulsive as well. In the Poisson–Boltzmann (PB) approximation, the counterion–counterion correlations are neglected, i.e. $g_{II}(r) \equiv 1$ with $g_{II}(r)$ denoting the counterion–counterion radial distribution function (rdf). In planar geometry, $g_{II}(r) \equiv 1$ implies $F_{elec}(r) \equiv 0$.

(4) There are an infinite number of ways to divide the mean force into two different components. This is a consequence of the freedom of selecting the surface of the surface integration of the stress tensor (see [17] and references given therein) to obtain the mean force. The conceptual merit of a particular choice is governed by the insight such a division can provide. Another division of $F(r)$ is obtained by insertion of equation (2) into (6), which splits equation (6) into one electrostatic contribution (*not* the same as the electrostatic term given in equation (10)) and one representing the net transfer of linear moments in the z direction arising from counterions colliding with the macroion [5, 9, 11, 13].

4. Simulation aspects

Two different and independent routes were used to determine the interaction between the macroions. The pmf acting between the two macroions was obtained directly by sampling the frequency of the macroion separation r, $P(r)$, from MC simulations of the model system in the canonical ensemble and using the relation

$$U^{pmf}(r)/kT = -\ln\left[\frac{P(r)}{P(r \to \infty)}\right]. \tag{12}$$

In practice, $P(L_{cyl}/2)$ was used to normalize $U^{pmf}(r)$, i.e. $U^{pmf}(L_{cyl}/2) \equiv 0$ was assigned. Since a regime with a high electrostatic coupling is considered, cluster movements strongly enhancing the simulation efficiently have been used [23]. In total 10^8 trial attempts per particle were applied, and translational displacement parameters 0.2–1.0 R_M for macroions and 0.1–0.5R_M for counterions were used.

In separate MC simulations with fixed positions of the macroions, $F_{ideal}(r)$ and $F_{elec}(r)$ were sampled separately according to equations (9) and (10) respectively, and $F(r)$ was subsequently obtained according to equation (8). These simulations were performed for macroion separations $r \leqslant R_F \equiv 2.975R_M$ in steps of $\Delta r = 0.050$. Each simulation involved 10^6 trial attempts per counterion, and similar displacement parameters as above were used. For $r < R_F$, $U^{pmf}(r)$ was also determined by integrating $F(r)$ according to equation (7). Since $F(r)$ was in most cases still nonzero at the integration limit R_F, these $U^{pmf}(r)$ were trivially shifted to agree with $U^{pmf}(r)$ determined from equation (12) at R_F. As seen in section 6, the two independent statistical–mechanical routes employing separate simulations to determine $U^{pmf}(r)$ were in excellent agreement with each other.

Uncertainties (one standard deviation) were evaluated by subdividing production runs into ten parts. The absolute uncertainties of $U^{pmf}(r)/kT$ evaluated from equation (12) were typically 0.01–0.02. At $r = 2.025R_M$ the absolute uncertainties of $F_{ideal}(r)/(kT/R_M)$ and $F_{elec}(r)/(kT/R_M)$ were typically 0.3 and 0.07 respectively (their relative uncertainties were typically 0.005 and 0.001 respectively), and at $r = 2.975R_M$ their absolute uncertainties were

0.03 and 0.005 respectively. The integrated MC/molecular dynamics/Brownian dynamics simulation package MOLSIM [24] for molecular systems was employed throughout.

5. Simple system at zero and infinite temperature limits

Before examining the simulation results, the foundation of an attractive interaction will first be demonstrated by using a simple system. Despite its simplicity, the system introduces the correct physics and has the advantage of possessing trivial analytic solutions in certain temperature limits.

Consider a system containing two macroions and four counterions with the macroion charge to counterion charge ratio $Z_r = 2$. The counterions are confined two by two to the surfaces of the two macroions, but otherwise they are mobile forming two subsystems each composed of one macroion and two counterions (the surface-constraint case). The limits of suppressed thermal fluctuations ($T = 0$ K) and of full surface fluctuations (infinite T) will be considered. At $T = 0$ K, the pmf between the two subsystems at the macroion separation r can be simplified, since no ensemble averaging is needed. Hence, $U^{pmf}(r)$ can be expressed as the change of the total potential energy of bringing the two subsystems from infinite separation to the separation r according to

$$U^{pmf}(r) = U(r; \{\boldsymbol{r}_I\}) - U(\infty; \{\boldsymbol{r}_I\}), \tag{13}$$

where $U(r; \{\boldsymbol{r}_I\})$ denotes that the total potential energy of the system, which, in addition to the separation r, also depends parametrically on the positions of the counterions $\{\boldsymbol{r}_I\}$.

Figure 1 displays the reduced pmf $U^{pmf\prime} \equiv U^{pmf}/(Z_I^2 e^2/4\pi\varepsilon_0\varepsilon_r R_M)$ at $r > 2R_M$ in the two temperature limits. At $T = 0$ K, a purely attractive interaction is observed, whereas at $T \to \infty$ the interaction $U^{pmf}(r)$ becomes identically zero after noting that all surface positions for the counterions are of equal probability. At $T = 0$ K and at infinite macroion separation, the two counterions in each subsystem are separated from each other by $2R_M$, and thus a subsystem possesses a quadrupole moment as the leading electrostatic multipole moment. When the two subsystems interact at a finite macroion separation, the counterions in one of the subsystems are located on the z axis joining the subsystems, whereas the other two counterions are off the z axis, as illustrated in the inset of figure 1. The inset also shows how the angle θ, describing the locations of the two counterions off the z axis, depends on r. The latter subsystem now possesses a dipole moment as the leading multipole moment, and the largest surface polarization appears at $r = 2R_M$, where $\theta(r)$–$\theta(\infty) = 13°$.

Thus, this simple system illustrates that at $T = 0$ K (i) an electroneutral Coulomb system displays a cohesive behaviour, (ii) the attraction can be viewed as originating from spatial correlations appearing between counterions residing at the different macroions, (iii) the subsystems are subjected to polarization because they possess internal degrees of freedom. At infinite temperature, the spatial correlation among the counterions residing at the different macroions has vanished and no attraction remains.

6. Macroions of higher net charge at finite temperature

The effective interaction between two macroions of higher net charge ($Z_r = 10$–40) in the presence of their counterions at finite, nonzero, temperatures will now be examined using the constrained and unconstrained cases. There are no (semi)analytic solutions to these conditions, and the results are obtained by MC simulations as described in section 4.

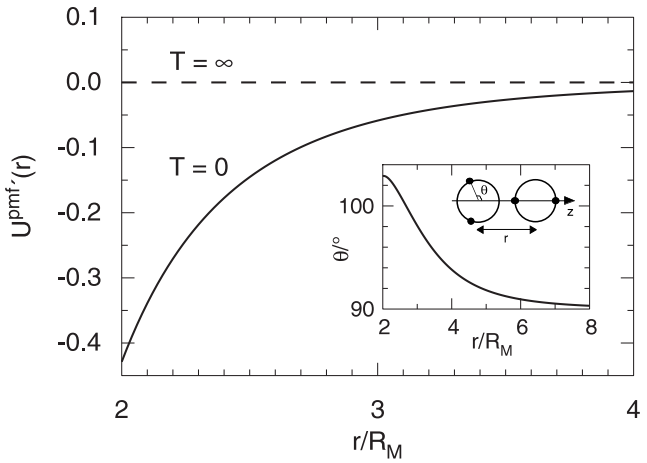

Figure 1. Reduced pmf [$U^{pmf\prime} \equiv U^{pmf}/(Z_I^2 e^2/4\pi\varepsilon_0\varepsilon_r R_M)$] as a function of the macroion separation (r) between two subsystems at $T = 0$ K (solid curve) and infinite T (dashed curve). Each subsystem contains one macroion and two counterions confined to the surface of the macroion but otherwise mobile. The inset illustrates the location of the counterions at $T = 0$ K and finite separation, and it also shows the angle (θ), describing the location of two of the four counterions, as a function of the macroion separation (r).

The charged particles are placed inside a hard cylindrical cell with radius R_{cyl} and length $L_{cyl} = 12R_M$. The electrostatic coupling parameter Γ_{II} will range from 1.067 to 1.779. It is recalled that the values of Γ_{II} selected are larger than those found in typical aqueous systems at ambient temperature with monovalent counterions, but are attainable with multivalent counterions and/or solvent with lower permittivity [19].

6.1. Constrained counterions, variation of Γ_{II}

A system having a macroion charge to counterion charge ratio $Z_r = 40$ at two values of the electrostatic coupling parameter Γ_{II} will be considered for the case of counterions constrained to the surfaces of the macroions. Figure 2 shows the mean force, its two components and the pmf as a function of the macroion separation r.

Figure 2(a) shows that the mean force $F(r)$ is attractive up to $r \approx 2.5R_M$, and its minimum appears at macroion contact. The attraction decreases as Γ_{II} is decreased, which is achieved, for example, by increasing T. The two components of $F(r)$ are shown in the inset of figure 2(a). In this case, $F_{ideal}(r)$ (diamonds) becomes trivially zero due to the fact that the counterions are confined to the surfaces of the macroions, whereas $F_{elec}(r)$ (circles) displays a short-range attraction. Since $F_{elec}(r) = 0$, $r > 2R_M$, would be obtained with $g_{II}(r) \equiv 1$, the attraction originates again from counterion correlations. Thus, it is solely the electrostatic correlations that contribute to $F(r)$ and make $F(r)$ attractive at short separation and approach zero from the attractive side.

The pmf $U^{pmf}(r)$ is shown in figure 2(b), and consequently it becomes negative at short macroion separation. The potential becomes less negative as Γ_{II} is decreased, and $U^{pmf}(r)$ amounts to a few kT at contact separation. In analogy with the simpler system dealt with in section 5, $U^{pmf}(r > 2R_M)$ will remain finite in the limit $\Gamma_{II} \to \infty$ (for example $T = 0$) and approach zero at $\Gamma_{II} = 0$ (for example $T \to \infty$). It is also observed that the two procedures for obtaining $U^{pmf}(r)$ provide numerically identical results (cf curves and symbols in figure 2(b)).

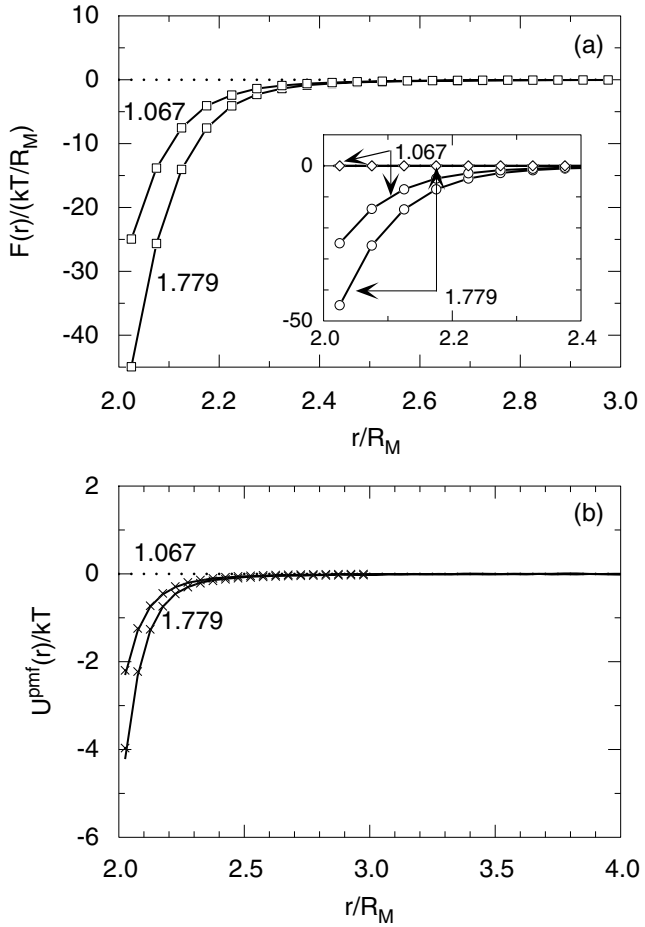

Figure 2. (a) Reduced mean force ($F(r)/(kT/R_M)$) (curves with squares) and its two components ($F_{ideal}(r)/(kT/R_M)$) (curves with diamonds) and ($F_{elec}(r)/(kT/R_M)$) (curves with circles) and (b) reduced pmf ($U^{pmf}(r)/kT$) (solid curves (equation (12)) and crosses (equations (7)–(10))) as a function of the macroion separation (r) for a system containing two macroions and their counterions, the latter constrained to the surfaces of the macroions, at $Z_r = 40$ and the indicated value of Γ_{II}.

Figure 3 displays typical snapshots at the macroion separation $r = 2.5R_M$ at the two Γ_{II} considered. Despite the strong electrostatic coupling, the counterions appear to form a two-dimensional fluid at the surfaces of the macroions. The surface structure is quantified in figure 4, showing the counterion–counterion rdfs using the arc length separation between pairs of counterions evaluated for a single macroion and its counterion. As for three-dimensional rdfs, $g_{II}^{surf}(r)$ is normalized to one for a uniform distribution, here for the counterions on the macroion surface. At short separation the counterions repel each other and at $\Gamma_{II} = 1.779 g_{II}^{surf}(r)$ displays a weak maximum at $r = 0.5R_M$, but beyond $r \approx R_M$ no surface structure remains. Thus, both the snapshots and $g_{II}^{surf}(r)$ show that the counterions form a fluid surface structure, even at the larger Γ_{II}, and it is concluded that a correlation attraction does not require a Wigner crystal arrangement, as is sometimes proposed.

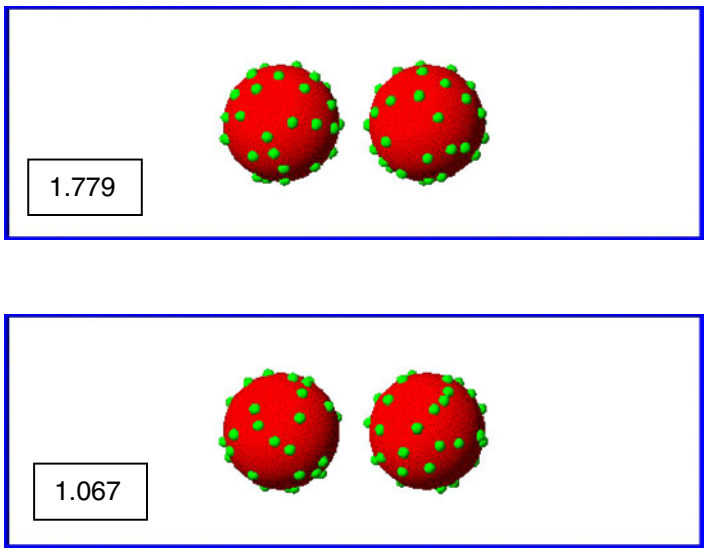

Figure 3. Snapshots of a system containing two macroions and counterions, the latter constrained to the surfaces of the macroions, enclosed in a cylindrical cell at macroion separation $r = 2.5R_M$ at $Z_r = 40$, $R_{cyl} = 2R_M$, $L_{cyl} = 12R_M$ and the indicated value of Γ_{II}. A small radius has been assigned to the point counterions to make them visible.

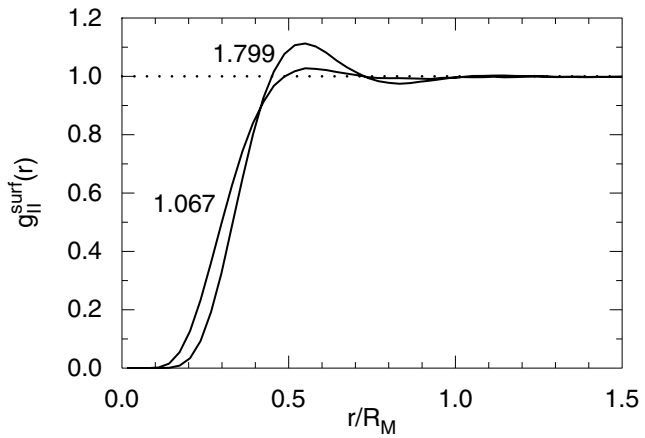

Figure 4. Counterion–counterion rdf ($g_{II}^{surf}(r)$) for a system containing one macroion and its counterions, the latter constrained to the surface of the macroion, at $Z_r = 40$ and the indicated value of Γ_{II}. Here, r denotes the arc length separation between pairs of counterions.

6.2. Unconstrained counterions, variation of Γ_{II}

The same investigation of the corresponding systems but with unconstrained counterions has been performed, and the (nearly) corresponding results are provided in figures 5–7. In addition, table 1 displays some selected data of $F(r)$ and the corresponding results for a different shape of the cylindrical cell.

Figure 5(a) displays the mean force at two different values of the electrostatic coupling parameter (same Γ_{II} as in figures 2–4). At the larger Γ_{II}, $F(r)$ possesses a short-range

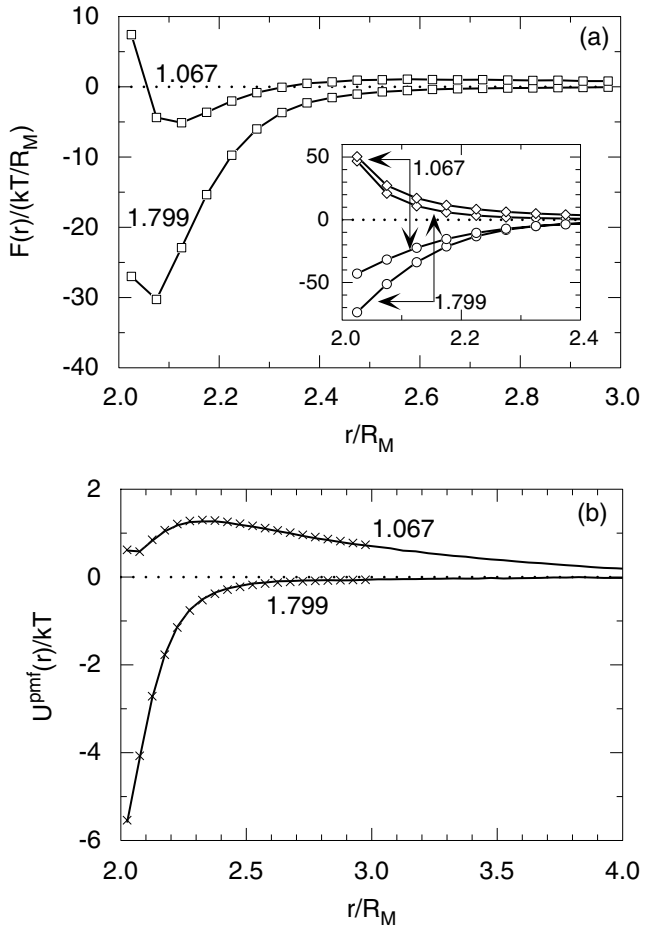

Figure 5. (a) Reduced mean force ($F(r)/(kT/R_M)$) (curves with squares) and its two components ($F_{ideal}(r)/(kT/R_M)$) (curves with diamonds) and ($F_{elec}(r)/(kT/R_M)$) (curves with circles) and (b) reduced pmf ($U^{pmf}(r)/kT$) (solid curves for equation (12) and crosses for equations (7)–(10)) as a function of the macroion separation (r) for a system containing two macroions and their counterions enclosed in a cylindrical cell at $Z_r = 40$, $R_{cyl} = 2R_M$, $L_{cyl} = 12R_M$ and the indicated Γ_{II}.

attraction with the strongest attraction slightly off contact and $F(r)$ approaches zero at $r \approx 3R_M$. However, at $\Gamma_{II} = 1.067$ a weak long-range repulsion appears and only at short separation does a region of an attractive force remain. At contact, the force becomes repulsive again. At even smaller Γ_{II}, the force becomes purely repulsive (data not shown).

The corresponding components of $F(r)$ are shown in the inset of figure 5(a). The ideal component $F_{ideal}(r)$ is repulsive and the magnitude of $F_{ideal}(r)$ *increases* and its range of interaction *increases* as Γ_{II} is decreased. At short macroion separation, the component $F_{elec}(r)$ is attractive, and the amplitude of $F_{elec}(r)$ *decreases* and the range of interaction is to the first order *unaffected* as Γ_{II} is decreased. These different Γ_{II}-dependences will make $|F_{ideal}(r)| > |F_{elec}(r)|$ for sufficiently small Γ_{II} at all r and $|F_{ideal}(r)| < |F_{elec}(r)|$ for the larger Γ_{II} considered at short separation. In the latter case, the decrease of $F_{elec}(r)$ becomes less than the increase of $F_{ideal}(r)$ at very short separation, making $F(r)$ display an upturn at these short macroion separations. Thus, at sufficiently high counterion charge, Bjerrum length or small macroion size, the electrostatic interaction will dominate over the ideal contribution

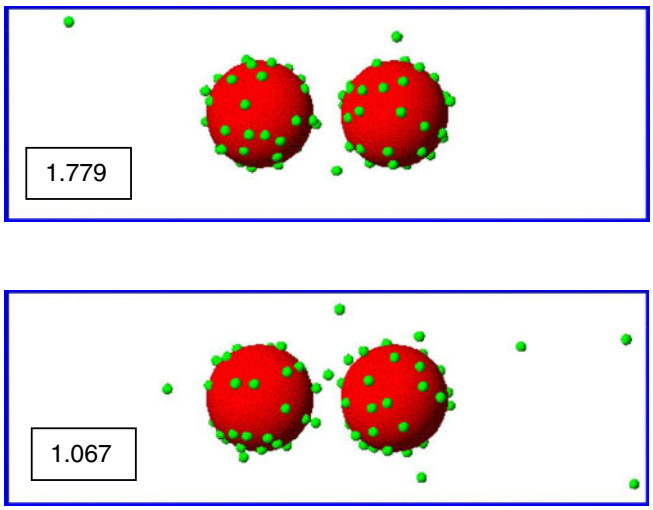

Figure 6. Snapshots of a system containing two macroions and counterions enclosed in a cylindrical cell at macroion separation $r = 2.5R_M$ at $Z_r = 40$, $R_{cyl} = 2R_M$, $L_{cyl} = 12R_M$ and the indicated Γ_{II}. A small radius has been assigned to the point counterions to make them visible.

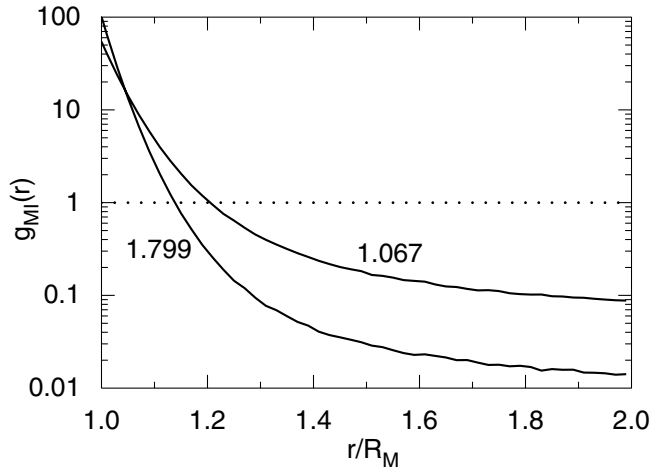

Figure 7. Macroion–counterion rdf ($g_{MI}(r)$) for a system containing one macroion and its counterions at $Z_r = 40$ and the indicated Γ_{II} enclosed in a spherical cell with radius $R_{sph} = 2R_M$.

giving rise to a short-range effective attraction as showed in figure 5, while in the other regime the electrostatic interaction is not sufficiently attractive. In the case where the counterion correlations are neglected, $g_{II}(r) \equiv 1$, still $F_{elec}(r) \neq 0$. Hence, $F_{elec}(r)$ contains both mean-field and counterion correlation contributions.

The pmfs of this system are shown in figure 5(b). As a consequence of the attractive $F(r)$ for $\Gamma_{II} = 1.779$, $U^{pmf}(r)$ is continuously decaying as r is decreased, and a minimum of $\approx 6kT$ appears at contact. At $\Gamma_{II} = 1.067$ with the richer mean force behaviour, the long-range repulsive mean force gives rise to a potential barrier of $\approx 1.2kT$ at $r \approx 2.3R_M$, and the attractive mean force at shorter separation results in a local free energy minimum of $\approx 0.8kT$

Table 1. Values of $F(r)$ at some selected r with $Z_r = 40$, $\Gamma_{II} = 1.067$ and two different cylindrical cell shapes but at the same volume $V = 48\pi R_M^3$.

	$F(r)/(kT/R_M)$	
r/R_M	$R_{cyl} = 2R_M$ $L_{cyl} = 12R_M$	$R_{cyl} = 2.449R_M$ $L_{cyl} = 8R_M$
2.025	$+7.4 \pm 0.3$	$+7.3 \pm 0.3$
2.075	-4.4 ± 0.2	-4.3 ± 0.2
2.125	-5.1 ± 0.1	-5.0 ± 0.1
...	...	...
2.475	$+0.94 \pm 0.05$	$+0.94 \pm 0.05$
...	...	...
2.975	$+0.81 \pm 0.03$	$+0.72 \pm 0.05$

at $r \approx 2.1R_M$. Again, two procedures of obtaining $U^{pmf}(r)$ evaluated from equations (12) and (7)–(10) agree completely.

The snapshots shown in figure 6 display that most of the counterions are electrostatically associated with the macroions. Nevertheless, some counterions explore the full cylindrical cell volume, and the number of detached counterions increases as Γ_{II} is reduced. The accumulation of the counterions near a macroion is described in more detail in figure 7, displaying macroion–counterion rdfs, $g_{MI}(r)$ evaluated from a single subsystem confined in a spherical cell. At macroion contact, the local counterion number density is about 100-fold larger than for a uniform distribution of the counterions in the spherical cell. The electrical double layer is thin (note, a logarithmic ordinate in figure 7), for example the contact densities are reduced 10-fold at the distances $r = 1.06$ and $1.14R_M$ for $\Gamma_{II} = 1.779$ and 1.067 respectively.

The constrained and unconstrained cases will now be compared. Obviously, $F(r)$ can display a qualitatively different behaviour for the two different conditions considered (cf curves with squares labelled $\Gamma_{II} = 1.067$ in figures 2(a) and 5(a)). In the unconstrained system, the release of the counterions makes the component $F_{ideal}(r)$ repulsive. Furthermore, the magnitude of the attractive $F_{elec}(r)$ is nearly two-fold larger (cf curves with circles in insets of figures 2(a) and 5(a)). At the *larger* Γ_{II}, the magnitude of the attractive $F(r)$ is still generally larger for the unconstrained system (despite $F_{ideal}(r) > 0$) (cf curves with squares labelled $\Gamma_{II} = 1.779$ in figures 2(a) and 5(a)). Thus, the additional degrees of freedom of the counterions can lead to a larger ability to establish electrostatically attractive configurations without sacrificing too much repulsion arising from the accumulation of counterions in between the macroions. However, at the *smaller* Γ_{II}, the thermal energy makes the electrical double layer sufficiently thick to establish an accumulation of counterions in the volume between the macroions, giving rise to a repulsive $F_{ideal}(r)$ comparable to the attractive $F_{elec}(r)$. At even smaller Γ_{II}, $|F_{ideal}(r)| > |F_{elec}(r)|$ and hence $F(r) > 0$ at all separations.

Finally, from the data given in table 1, it is observed that a reduction of the length of the cylindrical cell L_{cyl} by 1/3 and the concomitant increase of the radius of the cell R_{cyl}, keeping the volume fixed, does not alter the mean force within the numerical precision. The same negligible effect was found at $\Gamma_{II} = 1.799$. Hence, the exact shape of the cylindrical cell does not play a significant role under the present conditions.

6.3. Unconstrained counterions, variation of R_{cyl}

The mean force and the pmf between the two macroions with unconstrained counterions will now be examined at different cell volumes at an electrostatic coupling intermediate to those considered above.

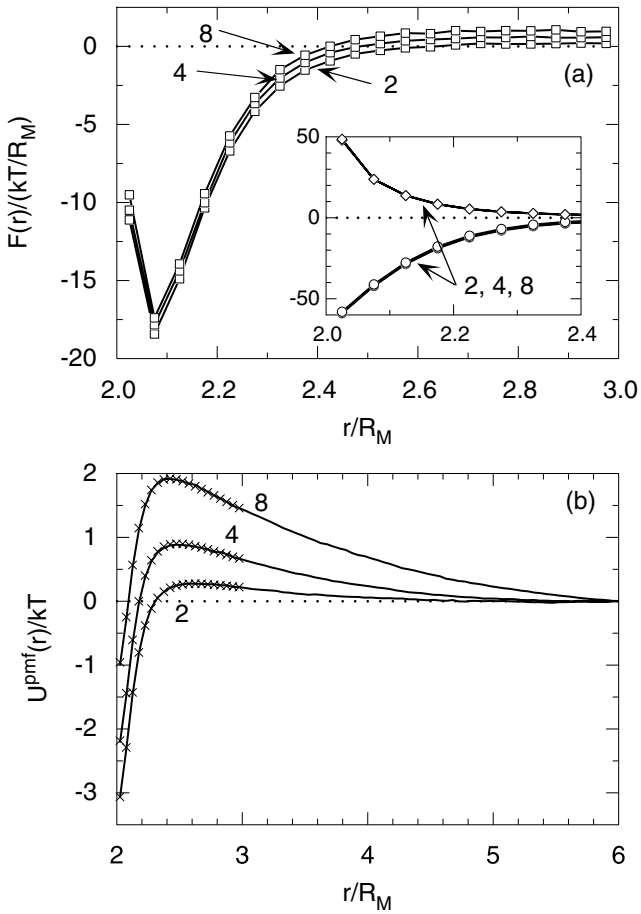

Figure 8. As figure 5, but at $Z_r = 40$, the indicated value of R_{cyl} and $\Gamma_{II} = 1.423$.

Figure 8(a) shows $F(r)$ at $\Gamma_{II} = 1.423$ at different cylinder volumes ($R_{cyl} = 2$, 4 and $8R_M$). The mean force curves display similar functional form, i.e. a long-range repulsion, a short-range attraction with the largest magnitude at $r \approx 2.1R_M$ and a weaker attraction at contact. At this intermediate Γ_{II}, $F(r)$ falls between $\Gamma_{II} = 1.067$ and 1.779 given in figure 5(a). In more detail, the short-range attraction becomes weaker and the long-range repulsion stronger as R_{cyl} is increased. The components of $F(r)$ are displayed in the inset of figure 8(a), and on this scale R_{cyl} has hardly any visible effect on them up to $r = 2.4R_M$. From an examination of $F_{ideal}(r)$ and $F_{elec}(r)$ in the interval $2.025R_M \leqslant r \leqslant 2.975R_M$ (the values at $r = 2.975R_M$ are given in table 2), it is found that $F_{ideal}(r)$ is insensitive to R_{cyl}, whereas $F_{elec}(r)$ increases significantly as R_{cyl} is increased, and that $F_{elec}(r)$ becomes *positive* at sufficiently large R_{cyl}.

The corresponding pmfs are reported in figure 8(b). Starting at $R_{cyl} = 2R_M$, only a weak long-range repulsion is present and a barrier of $\approx 0.3kT$ at $r/R_M \approx 2.4$ appears (cf figure 5(b)), whereas as R_{cyl} is increased the amplitude of the long-range repulsion increases and at the largest volume considered ($R_{cyl} = 8R_M$) the barrier has increased to $\approx 2kT$. The obvious interpretation is that an increase of the volume leads to a more extended double layer causing a stronger and more long-range repulsion. Grønbech-Jensen *et al* [10] have performed a related investigation and found similar behaviour of the pmfs.

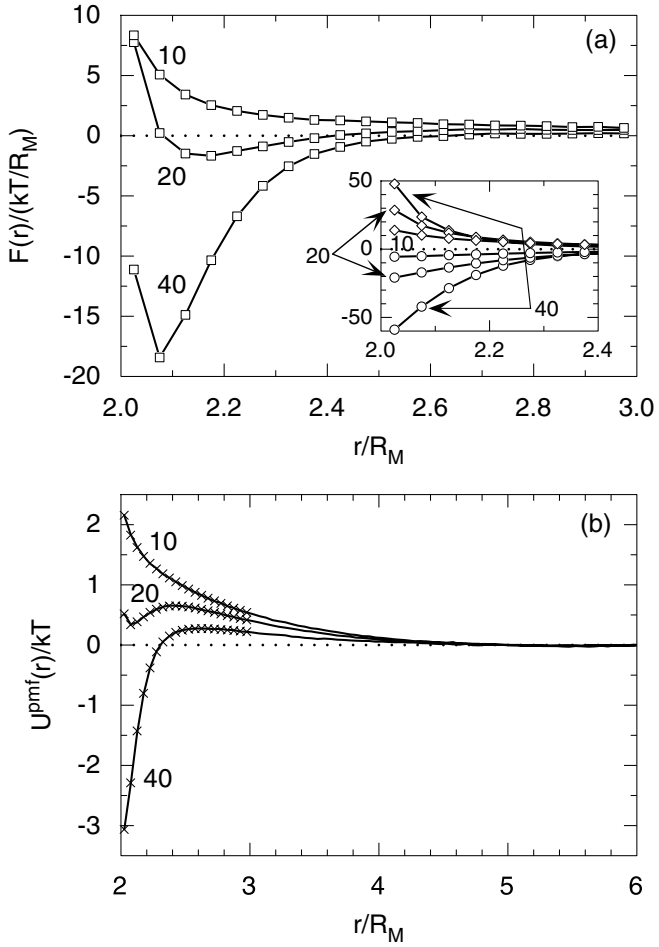

Figure 9. As figure 5, but at the indicated Z_r, $R_{cyl} = 2R_M$ and $\Gamma_{II} = 1.423$.

Table 2. Values of $F_{ideal}(r)$ and $F_{elec}(r)$ at $r = 2.975R_M$ with $Z_r = 40$, $\Gamma_{II} = 1.423$ and two different R_{cyl}.

R_{cyl}/R_M	$F_{ideal}(r)/(kT/R_M)$	$F_{elec}(r)/(kT/R_M)$
2	0.52 ± 0.02	-0.327 ± 0.005
4	0.63 ± 0.03	-0.048 ± 0.006
8	0.59 ± 0.03	$+0.373 \pm 0.006$

6.4. Unconstrained counterions, variation of Z_r

Finally, the effect of the macroion charge to counterion charge ratio Z_r on $F(r)$ and $U^{pmf}(r)$ at $\Gamma_{II} = 1.423$ and $R_{cyl} = 2R_M$ will be considered. Figure 9 presents the results for $Z_r = 10$, 20 and 40.

Starting with $Z_r = 40$, figure 9(a) shows again the weak long-range repulsive and the strong short-range attractive $F(r)$. When Z_r is reduced, for example by reducing the macroion charge Z_M, the effective attraction between the two macroions at short separation decreases.

At $Z_r = 20$ there is still a region of an attractive $F(r)$, whereas at $Z_r = 10$, $F(r)$ is purely repulsive. In addition, a long-range repulsive tail has emerged. Thus, upon an *increase* of their charges two repelling like-charged macroions may *start to attract* each other.

The inset of figure 9(a) shows that the magnitude of both $F_{ideal}(r)$ and $F_{elec}(r)$ increases strongly as Z_r is increased. Thus, for example, when the macroion charge is increased, the attractive electrostatic force as well as the more long-range ideal repulsion increases in importance. At the conditions employed, $|F_{elec}(r)|$ increases faster than $|F_{ideal}(r)|$ as Z_r is increased. Obviously, there is an intricate interplay between the ideal repulsion and the electrostatic attraction and their dependence on Z_r. It is recalled that the conditions at which $F_{elec}(r)$ and $F_{ideal}(r)$ approximately balance each other first appear at a reasonably large Γ_{II}. At a smaller Γ_{II}, the classical DLVO behaviour of a progressively more dominating repulsion as Z_r is increased would be recovered. Guldbrand *et al* and Kjellander and Marcelja have previously documented a similar finding of an attractive force between two like-charged planes as the surface charge densities of the planes are increased (see figure 5 of [5] and figure 2 of [6]). This attraction in planar geometry has recently been captured in the strong coupling regime by a recent theory by Moreira and Netz [25].

The corresponding pmfs are presented in figure 9(b). Whereas at $Z_r = 40$ a deep minimum of $\approx 3kT$ appears at contact, the pmf becomes repulsive with a metastable minimum at short separation at $Z_r = 20$, and finally a purely repulsive potential appears at $Z_r = 10$.

7. Discussion and conclusions

The mean force and the pmf between two macroions enclosed in a cylindrical cell together with their counterions have been determined by using MC simulations, which essentially provide the exact solution of the model considered. The system investigated is a simplification of a fluid of macroions and counterions. In particular, correlations involving three or more macroions are suppressed. The present study is focused on a region in the parameter space where short-range attraction starts to appear.

7.1. Relation to structure and phase behaviour of corresponding solutions

Simulations of the structure and the thermodynamics of the corresponding fluids employing a system containing 80 macroions and their counterions for an extended and connected region of the parameter space limited by $10 \leqslant Z_r \leqslant 80$, $0.001\,25 \leqslant \phi_M \leqslant 0.08$ and $0.0222 \leqslant \Gamma_{II} \leqslant 2.846$ have previously been performed [19]. At this level of description, macroion–macroion correlations beyond the pair correlations are included.

In a fluid, the pmf between particles i and j is directly obtained from their rdf according to $U^{pmf}_{fluid}(r)/kT \equiv -\ln[g_{ij}(r)]$. Hence, from the previous fluid simulations, pmfs between two macroions in the one-phase region are available. Figure 10 displays the deduced macroion–macroion pmfs $U^{pmf}_{fluid}(r)$ at $Z_r = 10$, 20 and 40, $\phi_M = 0.040$ and $\Gamma_{II} = 1.423$ (symbols) as well the corresponding $U^{pmf}(r)$ from the cylindrical cell model at identical Z_r and Γ_{II} but at somewhat larger $\phi_M = 2[(4\pi/3)R_M^3]/[\pi(2R_M)^2(12R_M)] = 0.056$ (curves). A comparison between $U^{pmf}_{fluid}(r)$ and $U^{pmf}(r)$ reveals a complete consistency of the main features. In particular, (i) the transition from a repulsive pmf at low Z_r to an attractive one at short separation at larger Z_r and (ii) the appearance of a long-range repulsion are noticeable. Thus, the salient features of the macroion–macroion pmf found in fluid simulations are well captured in the simplified cylindrical cell model containing two macroions and the relevant number of counterions only. A firmer inspection shows, however, that the cylindrical cell model overestimates the repulsion in the repulsive regime and overestimates the attraction when the

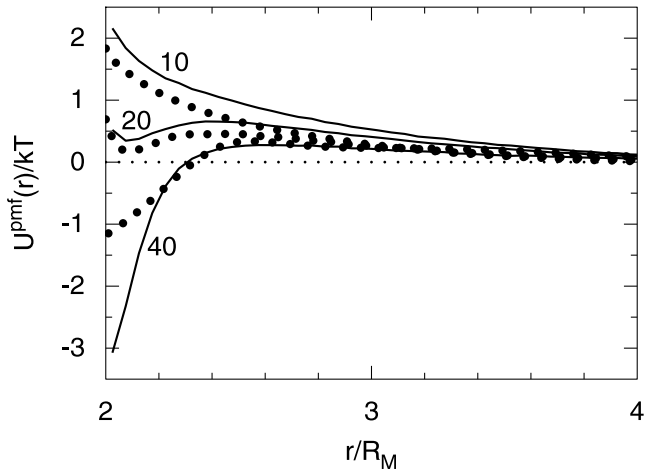

Figure 10. Reduced macroion–macroion pmf from a fluid system ($U^{pmf}_{fluid}(r)kT$) comprising 80 macroions and the corresponding number of counterions at $\phi_M = 0.040$ (symbols) and from the cylindrical cell model ($U^{pmf}(r)/kT$) (curves, data taken from figure 5) as a function of the macroion separation (r) at the indicated Z_r and $\Gamma_{II} = 1.423$. Here, $U^{pmf}_{fluid}(r)/kT \equiv -\ln[g_{MM}(r)]$ with g_{MM} denoting the macroion–macroion rdf ($g_{MM}(r)$ data from [19]).

attraction is dominating. Nevertheless, the structural effects of the higher-order macroion–macroion correlations included in the fluid simulations appear to be limited under the present conditions.

The pmf can also be related to the phase behaviour of the fluid systems. Figure 11 displays the binodal curve in the (Z_r, Γ_{II}) plane at $\phi_M = 0.01$ extracted from the fluid systems. At low Γ_{II}, a stable fluid characterized by conventionally repelling like-charged macroions was observed, whereas at $\Gamma_{II} \approx 1$–4 a gas–liquid phase separation occurs, signalling the existence of an effective attraction. The required Γ_{II} for the phase instability decreases as Z_r is increased. Figure 11 shows also the locations of some of the cylindrical cell systems investigated in the same (Z_r, Γ_{II}) plane. As mentioned, the macroion volume fraction of the latter systems is $\phi_M = 0.056$. Nevertheless, the disagreement in ϕ_M between the fluid and cell cases will not qualitatively affect our discussion, since the location of the binodal curve is only weakly dependent on ϕ_M in this regime (see figure 10(b) in [19]).

Considering first the variation in Γ_{II}. A very good agreement is found between the development of the short-range attraction showed in figure 5 and the approach to the binodal curve shown by arrow 1 in figure 11 as Γ_{II} is increased from 1.067 to 1.779 at $Z_r = 40$. Similarly, the appearance of a short-range attraction as Z_r is increased from 10 to 40 at $\Gamma_{II} = 1.423$ shown in figure 9 corroborates very well with the approach to the binodal curve displayed by arrow 2 in figure 11. Additional simulations with $Z_r = 10$ at $\Gamma_{II} > 1.423$ also displayed the appearance of an attractive force, for example at $\Gamma_{II} = 2.846$ a long-range repulsion with a barrier below $<0.1kT$ and a contact potential of $-2kT$ occurred, consistent with being near the binodal curve. Thus, there is very convincing agreement between the location of the binodal curve found from fluid simulations and the appearance of strong short-range attractions in the cylindrical cell model.

The strong consistency of the pmf obtained from the cylindrical cell model on the one hand and the pmf and the related phase instability of fluid systems on the other hand suggests that the cylindrical cell model should be an attractive method to assess, at least initially, the

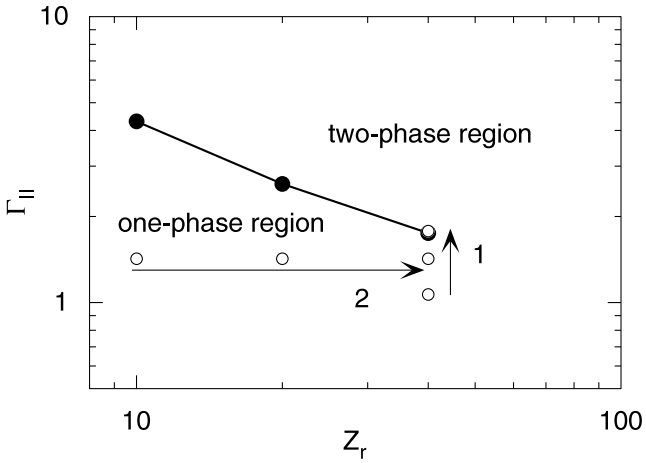

Figure 11. Binodal curve separating the regions with a stable one-phase fluid and the coexistence of two phases in the (Z_r, Γ_{II}) plane at $\phi_M = 0.01$ (curve) from fluid simulations (adapted from figure 10 of [19]) and the location in the (Z_r, Γ_{II}) plane of some of the cylindrical cell systems investigated here (open symbols). Arrows 1 and 2 illustrate a series of systems with increasing Γ_{II} and Z_r, respectively.

interaction between two macroions mediated by small ions within the primitive model. It should be noted that the computational effort between the fluid and cell approaches differs by about two orders of magnitude. This observation can be exploited to examine the interactions between like-charged colloids using the cylindrical cell approach in computationally more demanding cases. For example, (i) extending macroion charges to 1000–10 000 elementary charges corresponding to latex particles, (ii) describing the charges explicitly for explaining more complex macroions [26–28] and possibly making the surface charges mobile, and (iii) describing the effect of the surface polarization originating from different permeability of the interior of the macroions and the solution of the force between two macroions (the effects of surface polarization on the ion distribution near one macroion has been examined [29, 31]).

7.2. Nature of short-range attraction

The mean force was divided into two contributions, of which one is related to the difference of the counterion density in the mid-plane of the macroions at the cylinder ends and the other to the electrostatic interaction across the mid-plane. It should be clear that the former term depends on the electrostatic interactions indirectly. At short macroion separation, the ideal contribution to the mean force is bound to be repulsive in the present type of systems. The contribution from the electrostatic interaction can be both negative and positive, although the former was found nearly exclusively under the present conditions.

When the mean force is purely repulsive, the ideal contribution dominates at all separations. However, as Γ_{II} is increased, the contribution from the electrostatic interaction becomes larger in magnitude than the ideal contribution starting at short separation. Finally, at sufficiently large Γ_{II}, the mean force is in practice attractive at all separations. Similar changes in the mean force appear as the macroion density is decreased or as the macroion charge to counterion charge ratio is increased. This qualitative change of the mean force as Γ_{II}, ϕ_M and Z_r is changed, as displayed in figures 5, 8 and 9 respectively, is a consequence of small changes in

the two components of the mean force. Hence, there are no qualitative changes in the molecular arrangement at the onset of the attraction.

The mean force can formally and conceptually *also* be divided into one (mean-field) double-layer force and one contribution arising from the correlation among the counterions. The (mean-field) double-layer force would contain (i) the ideal force contribution and (ii) the contribution from the electrostatic interaction in a description where *the counterion–counterion correlations are neglected* ($g_{II}(r) \equiv 1$) and has been shown to be repulsive at all separations, see [32, 33] for analytic proof. For the systems with surface-constrained counterions, the double-layer repulsion was artificially suppressed and only the remaining counterion–counterion correlations came into action. The even simpler system dealt with in section 5 possessed an analytical pmf at zero temperature. Thus, (for the unconstrained systems) it is concluded that (i) the attraction observed originates from the correlation of counterions residing at different macroions and (ii) the attractive force appears when the double-layer repulsion becomes sufficiently short range such that the magnitude of the attractive counterion–counterion correlation is able to become the dominating contribution.

Finally, in the present investigation point counterions have been employed. The results presented remain qualitatively the same for counterions possessing a radius typical for simple ions. The main qualitative difference is that the rise of the mean force and of the pmf is shifted from $2R_M$ to $2(R_M + R_I)$, where R_I is the radius of the counterion [21]. However, at a larger counterion size, the mean force and pmf become affected by the size of the counterions [22].

Acknowledgments

Generous and valuable discussions with Roland Kjellander and Håkan Wennerström are gratefully acknowledged.

References

[1] Derjaguin B V and Landau L 1941 *Acta Physiochim. (USSR)* **14** 633
[2] Verwey E J and Overbeek J T G 1948 *Theory of the Stability of Lyophobic Colloids* (Amsterdam: Elsevier)
[3] Oosawa F 1968 *Biopolymers* **6** 1633
[4] Oosawa F 1971 *Polyelectrolytes* (New York: Dekker)
[5] Guldbrand L, Jönsson B, Wennerström H and Linse P 1984 *J. Chem. Phys.* **80** 2221
[6] Kjellander R and Marcelja S 1984 *Chem. Phys. Lett.* **112** 49
[7] Guldbrand L, Nilsson L G and Nordenskiöld L 1986 *J. Chem. Phys.* **85** 6686
[8] Woodward C, Jönsson B and Åkesson T 1988 *J. Chem. Phys.* **89** 5145
[9] Allahyarov E, D'Amico I and Löwen H 1998 *Phys. Rev. Lett.* **81** 1334
[10] Grønbech-Jensen N, Beardmore K M and Pincus P 1998 *Physica* A **261** 74
[11] Wu J, Bratko D and Prausnitz J M 1998 *Proc. Natl Acad. Sci. USA* **95** 15169
[12] Linse P and Lobaskin V 1999 *Phys. Rev. Lett.* **83** 4208
[13] Wu J, Bratko D, Blanch H W and Prausnitz J M 1999 *J. Chem. Phys.* **111** 7084
[14] Jönsson B and Wennerström H 2001 *When Ion–Ion Correlations are Important in Charged Colloidal Systems* ed C Holm, P Kékicheff and R Podgornik (London: Kluwer Academic)
[15] Kjellander R and Marcelja S 1988 *J. Chem. Phys.* **88** 7138
[16] Vlachy V 1999 *Annu. Rev. Phys. Chem.* **50** 145
[17] Belloni L 2000 *J. Phys.: Condens. Matter* **12** R549
[18] Hansen J-P and Löwen H 2000 *Ann. Rev. Phys. Chem.* **51** 209
[19] Linse P 2000 *J. Chem. Phys.* **113** 4359
[20] Linse P 2001 *Phil. Trans. R. Soc.* A **359** 853
[21] Lobaskin V, Lyubartsev A and Linse P 2001 *Phys. Rev.* E **63** 020401
[22] Kjellander R and Marcelja S 1986 *J. Phys. Chem.* **90** 1230
[23] Lobaskin V and Linse P 1999 *J. Chem. Phys.* **111** 4300
[24] Linse P 2002 *MOLSIM* Lund University, Sweden

[25] Moreira A G and Netz R R 2001 *Phys. Rev. Lett.* **87** 078301
[26] Allahyarov E, Löwen H, Louis A A and Hansen J P 2002 *Europhys. Lett.* **57** 731
[27] Messina R 2002 *Physica* A **308** 57
[28] Striolo A, Bratko D, Wu J Z, Elvassore N, Blanch H W and Prausnitz J M 2002 *J. Chem. Phys.* **116** 7733
[29] Linse P 1986 *J. Phys. Chem.* **90** 6821
[30] da Silva F L B, Bogren D, Söderman O, Åkesson T and Jönsson B 2002 *J. Phys. Chem.* B **106** 3515
[31] Messina R 2002 *J. Chem. Phys.* at press
[32] Neu J C 1999 *Phys. Rev.* E **82** 1072
[33] Sader J E and Chan D Y C 1999 *J. Colloid Interface Sci.* **203** 268